Received: 22 December 2017 | Revised: 13 July 2018 | Accepted: 16 July 2018

DOI: 10.1002/eco.2015

RESEARCH ARTICLE

WILEY

Applying the eco-hydrological equilibrium hypothesis to model root distribution in water-limited forests

Antoine Cabon[1,2] | Jordi Martínez-Vilalta[2,3] | Juan Martínez de Aragón[1] | Rafael Poyatos[2,4] | Miquel De Cáceres[1,2]

[1] Forest Science and Technology Centre of Catalonia (CEMFOR-CTFC), Solsona, Spain

[2] CREAF, Cerdanyola del Vallès, Barcelona, Spain

[3] Universitat Autònoma de Barcelona (UAB), Barcelona, Spain

[4] Laboratory of Plant Ecology, Faculty of Bioscience Engineering, Ghent University, Ghent, Belgium

Correspondence
Antoine Cabon, Centre Tecnològic Forestal de Catalunya, Carretera de Sant Llorenç de Morunys km 2, Solsona E-25280, Spain.
Email: antoine.cabon@ctfc.es

Funding information
Spanish Ministry of Economy and Competitiveness, Grant/Award Numbers: AGL2015-66001-C3-1-R, BES- 2015-071350, CGL2013-46808-R, CGL2014-5583-JIN, CGL2014-59742-C2-2-R and RYC-2012-11109

Abstract

Drought is a key driver of vegetation dynamics, but plant water-uptake patterns and consequent plant responses to drought are poorly understood at large spatial scales. The capacity of vegetation to use soil water depends on its root distribution (RD). However, RD is extremely variable in space and difficult to measure in the field, which hinders accurate predictions of water fluxes and vegetation dynamics. We propose a new method to estimate RD within water balance models, assuming that vegetation is at eco-hydrological equilibrium (EHE). EHE conditions imply that vegetation optimizes RD such that transpiration is maximized within the limits of bearable drought stress, characterized here by species-specific hydraulic thresholds. Optimized RD estimates were validated against RD estimates obtained by model calibration from sap flow or soil moisture from 38 forest plots in Catalonia (NE Spain). In water-limited plots, optimized RD was similar to calibrated RD, but estimates diverged with higher water availability, suggesting that the EHE may not be assumed when water is not limiting. Thereafter, we applied the optimization procedure at the regional scale, to estimate RD for the water-limited forests of Catalonia. Regional variations of optimum RD reproduced many expected patterns in response to climate, soil physical properties, forest structure, and species hydraulic traits. We conclude that RD optimization, based on the EHE hypothesis and a simple description of plant hydraulics, produces realistic estimates of RD that can be used for model parameterization and shows promise to improve our ability to forecast vegetation dynamics under increased drought.

KEYWORDS

eco-hydrological equilibrium, modelling, plant hydraulics, root distribution, transpiration, water balance

1 | INTRODUCTION

Water availability is a key ecological factor to understand vegetation growth, mortality, and regeneration. As global temperatures are projected to increase, and despite the uncertainty in predicted shifts of precipitation patterns, longer and more intense droughts are expected to occur and shape future vegetation dynamics in many regions of the world (IPCC, 2014). However, understanding how drought affects vegetation dynamics requires an accurate characterization of the hydric environment experienced by plants (Anderegg, Anderegg, & Berry, 2013).

Climatic aridity is correlated to broad-scale variations in vegetation characteristics (Grier & Running, 1977; Schulze et al., 1996) and to dynamic responses, such as tree growth (Andreu et al., 2007; Brienen & Zuidema, 2005; Sarris, Christodoulakis, & Körner, 2007). However, because the soil acts like a buffer of the water regime

imposed by climate, quantifying edaphic drought gives more insights than climatic variables alone when assessing ecological patterns such as tree growth (Bréda, Granier, & Aussenac, 1995; Manrique-Alba et al., 2017), fire occurrence (Taufik et al., 2017), species distributions (Le Roux, Aalto, & Luoto, 2013; Piedallu, Gégout, Perez, & Lebourgeois, 2013), or water availability with climate change (Tietjen et al., 2017). The eco-hydrological processes affecting soil water dynamics (i.e., precipitation interception, run-off, deep drainage, and evapotranspiration) are largely determined by the soil–plant-available water holding capacity (sensu Donohue, Roderick, & McVicar, 2012; Smettem & Callow, 2014) and vegetation properties. Among vegetation properties, the vertical root distribution (RD) in the soil and particularly, the ability of plants to produce deep roots determine the plants' water extraction profile and actual experience of edaphic drought (Anderegg et al., 2013; Federer, Vörösmarty, & Fekete, 2003; Gardner, 1964; Jackson et al., 1996; Rodriguez-Iturbe, Porporato, Ridolfi, Isham, & Cox, 1999; Zeng, Dai, Dickinson, & Shaikh, 1998). Field studies have shown that co-occurring species with contrasting rooting depths can exhibit very different water status (Bucci, Scholz, Goldstein, Meinzer, & Arce, 2009; Nardini et al., 2016; Stahl et al., 2013), which is linked with plants' ability to cope with drought (Nardini et al., 2016; Padilla & Pugnaire, 2007; Pinheiro, DaMatta, Chaves, Loureiro, & Ducatti, 2005). Moreover, RD is highly variable from local to global scales (Canadell et al., 1996; Jackson et al., 1996; Schenk & Jackson, 2002a; Stone & Kalisz, 1991), and this variability is integral part of plants' response to different environmental conditions (Hamer, Veneklaas, Renton, & Poot, 2016; Hartmann & von Wilpert, 2014; Kirchen et al., 2017; Schmid & Kazda, 2002).

Its functional importance and high diversity make RD a critical parameter to integrate within vegetation models. However, RD parameterization is considerably hindered by the difficulty to directly observe roots and the limited amount of field data, especially at large spatial scales. As a consequence, various methodologies have been developed to estimate RD (for a synthetic review, see Wang-Erlandsson et al., 2016). One approach consists in building empirical models that take into account interspecific variability and environmental factors to interpolate RD (Schenk & Jackson, 2002a, 2002b; Fan, Miguez-Macho, Jobbágy, Jackson, & Otero-Casal, 2017). However, accounting for the large number of factors that affect RD requires intensive measurements and large datasets for model calibration, whereas models that include a limited number of factors may have low predictive capacity, especially at local scales. Alternatively, RD can be estimated indirectly from ecological or hydrological data, such as ecosystem production or evapotranspiration, by retrieving RD for which the observed patterns are most likely (e.g., by a mass balance approach; de Boer-Euser, McMillan, Hrachowitz, Winsemius, & Savenije, 2016; Gao et al., 2014) or that maximizes model fit against observations (inverse modelling and calibration approaches; Ichii et al., 2007; Kleidon, 2004). However, estimates derived by these methods are data dependent and generally do not give insights on the actual drivers of RD (Wang-Erlandsson et al., 2016). Another approach to estimate RD consists in hypothesizing an ecological optimum (optimization approach), which is typically considered to be reached when vegetation properties yield maximized primary production (or minimized carbon cost; Kleidon & Heimann, 1998; Schymanski, Sivapalan, Roderick, Beringer, & Hutley, 2008) or water use (or minimized drought stress; Collins & Bras, 2007; van Wijk & Bouten, 2001) under given environmental conditions. Such optimality-based methods have the potential to explain current RD patterns and predict their future dynamics but nonetheless raise the question of determining what criterion to optimize.

The EHE hypothesis (Eagleson, 1982) is based on the concept of ecological optimality. In its original formulation, the EHE states that, in a given edaphic and climatic environment, canopy density and species composition tend to equilibrate towards an optimal hydric state that is assumed to be attained through a minimization of vegetation drought stress. An ecologically sounder hypothesis is that it is rather a trade-off between vegetation water use and drought stress that drives vegetation towards the EHE (Caylor, Scanlon, & Rodriguez-Iturbe, 2009; Kerkhoff, Martens, & Milne, 2004). Various studies have indeed reported relationships between canopy density and water availability (Grier & Running, 1977; Joffre, Rambal, & Ratte, 1999; Schulze et al., 1996) or between water availability and plant hydraulic properties (Brodribb & Hill, 1999; Choat et al., 2012; Choat, Sack, & Holbrook, 2007), and the concept of EHE, based on a trade-off between water use and water stress, has proved successful to explain spatial and temporal variations in vegetation patterns (e.g., structure and canopy density; Caylor et al., 2009; Hoff & Rambal, 2003; Kergoat, 1998; Nemani & Running, 1989).

Recent advances in the field of plant hydraulics help understanding plant drought stress on a mechanistic basis, which could substantially improve the way the trade-off between water use and drought stress is conceptualized within the EHE framework. There is growing consensus that hydraulic failure is the main physiological mechanism explaining plants' vulnerability to drought (Adams et al., 2017). Consistently, with the hypothesis that plants operate near their point of catastrophic hydraulic failure (Tyree & Sperry, 1988), Choat et al. (2012) reported that most forest species worldwide operate with narrow hydraulic safety margins (i.e., the difference between the minimum water potential and the water potential inducing hydraulic failure), independently from climatic water availability. This evidence suggests that plant vulnerability to embolism is a physiologically meaningful measure of drought tolerance and that it can mechanistically explain ecological patterns (Brodribb, 2017; Larter et al., 2017), such as forest die-off (Allen et al., 2010; Anderegg et al., 2016) or species distribution (Brodribb & Hill, 1999; Cosme, Schietti, Costa, & Oliveira, 2017; Pockman & Sperry, 2000). The use of a robust drought stress index based on plant hydraulics together with the concept of EHE therefore is of great promise for the estimation of plants' RD and improving the modelling of water and vegetation dynamics.

Here, we apply this theoretical framework to estimate the parameters of RD within a water balance model that simulates water fluxes based on meteorology, vegetation structure and soil data, and a synthetic description of plant hydraulics. Species-specific RD is estimated by optimizing rooting depth (Z) and the fine root proportion (FRP) in each soil layer such that the species annual transpiration is maximized, whereas plant minimum water potential is constrained to values close to the point of catastrophic xylem failure. We use experimental forest plots and national forest inventory data from Catalonia (NE Spain) to address the following specific objectives:

1. Quantifying the sensitivity of modelled forest transpiration to RD.
2. Testing the usefulness of the EHE hypothesis together with a simple plant hydraulics-based description of drought stress to parameterize RD, under a range of situations, including variation in soil and climate conditions, forest composition, and forest structure.
3. Analysing the factors driving the regional variations of RD estimates derived from the EHE hypothesis.

2 | MATERIAL AND METHODS

2.1 | Study area

The forested area (canopy cover >5%) of Catalonia (north-eastern Spain) covers 1.2 million ha and accounts for 38% of the territory (Ibàñez & Burriel, 2010, Figure 1). Catalan forests distribution spans from the Mediterranean coast to the Pyrenean Mountains (Figure 1). This area is characterized by a strong climate gradient, from Mediterranean to alpine. The mean annual temperature ranges between 0°C and 17.3°C (12.3°C on average). Annual precipitations are 727 mm on average and range between 335 and 1,593 mm. There is a strong spatial variation in seasonality of precipitations, but on average, February is the driest month (39 mm), followed by July (42 mm), whereas October (80 mm) and May (79 mm) are the wettest (Ninyerola, Pons, & Roure, 2000).

The vast majority (98%) of the Catalan forested area is composed of dense forests (canopy cover >20%). Coniferous species dominate 60% of the Catalan forest area, whereas 26% is dominated by broadleaf sclerophyllous species, 10% by broadleaf winter deciduous species, and the remaining 4% are mixed forests (Gracia, Ibàñez, Burriel, Mata, & Vayreda, 2004). Ranked by occupied area, the main tree species are *Pinus halepensis* Mill. (Aleppo pine), *Pinus sylvestris* L. (Scots pine), *Quercus ilex* L. (holm oak), *Pinus nigra* Arnold (black pine), *Quercus pubescens* Willd. (downy oak), *Quercus suber* L. (cork oak), *Pinus uncinata* Ram. (mountain pine), *Pinus pinea* L. (Italian stone pine), *Fagus sylvatica* L. (European beech), *Pinus pinaster* Aiton (maritime pine), and *Abies alba* Mill. (silver fir).

2.2 | Forest inventory data

The Third Spanish Forest Inventory (SFI3) surveyed over 10,000 forest plots in Catalonia between 2000 and 2001 (Figure S3A), distributed following a 1-km systematic grid. For each plot, the species identity, the diameter at breast height (DBH), and tree height were recorded within the area delimited by concentric circles of radius 5, 10, 15, and 25 m for standing trees (living and dead) with a DBH larger than 7.5, 12.5, 22.5, and 42.5 cm, respectively. The number of saplings per species and their mean height were estimated within the subplot of 5-m radius. Additionally, the cover and mean height of each understory woody species were estimated within the subplot of 10-m radius.

2.3 | Soil water content and sap flow measurements

Soil water content (SWC) or sap flow were monitored at 39 additional experimental plots (Table 1). Sap flow measurements were conducted at the Poblet Forest Natural Reserve in the Prades Mountains (Titllar Valley; 41°19′N, 1°00′E; 990–1,090 m a.s.l.). In this area, drought-

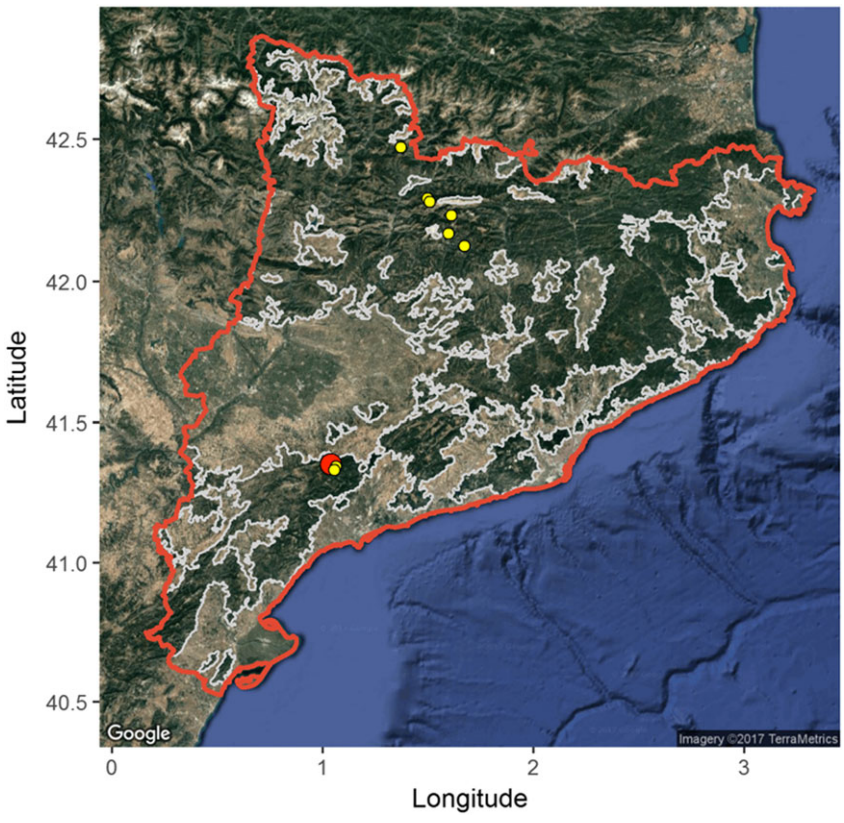

FIGURE 1 Satellite view of Catalonia (NE Spain) displaying the Catalan administrative boundary in red. The boundaries of Catalan forest area as defined by Ibàñez and Burriel (2010) are represented in grey. The location of the Poblet Forest Natural Reserve is shown by the red dot. Yellow dots indicate the position of the eight *P. sylvestris* plots where soil water content was monitored in 2016. The maps were obtained using satellite images from Google (Imagery: TerraMetrics) using the R package "ggmap"

TABLE 1 Main characteristics of the experimental plots where sap flow or SWC were monitored

Measurement	Source	Main species	Number. of plots	Time period	LAI	MAP (mm)	MAT (°C)	Remark
Sap flow	Aguadé et al., 2015	*Q. ilex/P. sylvestris*	1	2010–2011	2.69/0.58	527	11.7	−/drought-induced defoliation gradient
		Q. ilex	1	2010–2011	4.59	527	11.7	
		P. sylvestris	1	2010–2011	0.91	527	12.1	drought-induced defoliation gradient
SWC	Karavani et al., 2018	*P. pinaster*	28	2013–2014	1.04–3.67	663–792	9.3–13.0	Altitudinal and density gradient
	This study	P. sylvestris	8	2016	1.21–2.51	479–624	10.2–15.0	Climatic gradient

Note. Mean annual precipitation (MAP) and mean annual temperature (MAT) were calculated for the time period corresponding to the measurements. LAI: Leaf area index.

related defoliation and mortality events have been observed since the 1990s on *P. sylvestris*, which is progressively being replaced by *Q. ilex* as the dominant species (Poyatos, Aguadé, Galiano, Mencuccini, & Martínez-Vilalta, 2013). Sap flow was measured continuously (at 15-min intervals, aggregated at the daily scale) on 51 trees in total, which were divided in three plots (one pure pine stand, one pure oak stand, and one mixed stand; 10 trees in each pure stand and 31 in the mixed stand), using one to two constant heat dissipation sensors per tree. Stand transpiration was obtained by multiplying mean sap flow per unit of sapwood area for each species by the corresponding stand sapwood areas derived from site-specific allometries (Aguadé, Poyatos, Rosas, & Martínez-Vilalta, 2015; Poyatos et al., 2013).

A first set of SWC measurements was conducted at 28 plots (Karavani, De Cáceres, Martínez de Aragón, Bonet, & De-Miguel, 2018) located in 60-year-old *P. pinaster* plantation, across an elevation gradient in the Poblet Forest Natural Reserve (41°21′N, 1°2′E; 594–1,013 m a.s.l). Among the 28 *P. pinaster* plots, 13 were thinned in 2009 with different levels of thinning intensity (ranging between 26% and 77% decrease in basal area; Bonet, De-Miguel, Martínez de Aragón, Pukkala, & Palahí, 2012). Overall, the sampled *P. pinaster* plots therefore exhibited a large range of canopy density (Table 1).

A second set of SWC measurements was carried out at eight *P. sylvestris* plots representing the extent of *P. sylvestris* distribution in Catalonia, from the Prades Mountain in the south to the Pyrenees in the North. The resulting plots showed a strong climatic gradient (Table 1).

In all the 36 plots where SWC was monitored, SWC was consistently measured using one Decagon 5 TM probe (Decagon devices Inc., USA) per plot, placed in the middle of each plot, 12–15 cm belowground. Measurements were recorded every minute and averaged daily.

2.4 | Meteorological data

Daily meteorological data (minimum and maximum temperature, precipitation, and wind speed) were compiled for the 1995–2016 period from the surface weather stations network of the Spanish and Catalan meteorological services, within an area that comprised Catalonia and the surroundings. The total number of daily observations (Catalonia and surrounding Spanish regions) was on average 298 for temperature, 406 for precipitation, and 51 for wind speed. Interpolation of meteorology by taking into account topography as well as the calculation of daily potential evapotranspiration (Penman, 1948) for each study plot (i.e., SFI3 and experimental plots) was done using the R package "meteoland" (De Cáceres, Martin-StPaul, Turco, Cabon, & Granda, 2018; Figure S4A,B).

2.5 | Leaf area index

At the plots where sap flow measurements were conducted, tree leaf area (projected) was estimated from their DBH using equations calibrated on-site (Ogaya i Inurrigarro, 2004; Poyatos et al., 2013) and used to calculate leaf area index (LAI). In all the other forest plots (SWC plots and SFI3 plots), LAI of trees was derived for each species from their DBH and the total basal area of larger (BAL) trees in the plot, to account for asymmetric competition effects, as

$$\mathrm{LAI} = 1/S \cdot \mathrm{SLA} \cdot \sum_i a \cdot \mathrm{DBH}_i^b \cdot e^{c\mathrm{BAL}_i} \cdot \mathrm{DBH}_i^{d\mathrm{BAL}_i}, \quad (1)$$

where *i* is the target tree, SLA is the specific leaf area of the species considered, *S* the plot surface, and *a*, *b*, *c*, and *d* are species-specific parameters calibrated against measurements from Gracia et al. (2004; across all plots and species $R^2 = 0.72$). Additionally, because allometries were not available for shrubs, their LAI was estimated at the SFI3 plots by assuming a proportional relationship between LAI and shrub cover (Balandier et al., 2013), with a factor of 0.01. Total plot LAI was calculated as the sum of the trees and shrubs LAI (Figure S4C).

2.6 | Water balance model

The water balance model described in De Cáceres et al. (2015; implemented in the R package "medfate") was used to simulate vertical water fluxes and estimate plant drought stress for each plot. Stand structure is represented by plant height and LAI. Plants of a same species and of similar size are lumped into cohorts, although the definition of cohort is flexible in the model. The model follows the design principles from BILJOU (Granier, Bréda, Biron, & Villette, 1999) and SIERRA water balance submodel (Mouillot, Rambal, & Lavorel, 2001). The model runs start at the beginning of the year with the SWC at full capacity and performs daily updates of SWC as a function of the stand structure and daily weather (radiation, temperature, and precipitation). The soil water balance is the difference between infiltration (i.e., precipitation minus canopy interception and surface run-off) and the different water outputs: deep drainage, bare soil evaporation, and plant

transpiration. Maximum daily transpiration (E_{max}) is a function of LAI and PET as defined by Granier et al. (1999) and the actual daily transpiration (E) is the product between E_{max} and the whole-plant relative hydraulic conductance (G, see below). Further details on the formulation of each of these processes are given in De Cáceres et al. (2015).

The total soil depth (D) was divided into two layers: the topsoil (0–300 mm) and the subsoil (300 − D mm). Each soil layer was attributed a texture, described by the percentage of sand, loam, and clay, as well as a rock fragment content (RFC), which were derived from the Harmonized World Soil Database and the SFI3 inventory, respectively. RD was described at the species level by the rooting depth (Z), which equals D in the mono-specific case and by the FRP in each soil layer.

The water balance model was used to simulate daily values of E and G. The latter is calculated as the average of plant's relative hydraulic conductance in each soil layer (G_k) weighted by FRP:

$$G = \sum_k G_k \cdot FRP_k \quad (2)$$

G_k is derived from the water potential (Ψ) of the kth soil layer using a sigmoidal function:

$$G_k = \exp\left\{ \ln(1/2) \cdot \left(\frac{\Psi_k}{\Psi_{extract}} \right)^3 \right\}, \quad (3)$$

where $\Psi_{extract}$ is a species-specific parameter controlling the value of Ψ at which G_k equals 50% of its maximal potential value. Any conductance loss is assumed to be reversible. The daily plant water potential (Ψ_{plant}) is then calculated from G by inverting Equation (3), which does not account for the drop in water potential within the plant.

In this study, the yearly minimum plant water potential (Ψ_{min}) is defined at the cohort level as the average of Ψ_{plant} during the driest 10 consecutive days of the year. We also define the percentage of loss of conductance (PLC) as the complementary of G, and PLC_{max} as the average of PLC during the driest 10 consecutive days of the year.

2.7 | Optimization of RD parameters according to the eco-hydrological equilibrium hypothesis

The eco-hydrological equilibrium (EHE) hypothesis states that under given climate and edaphic conditions, the stand LAI will tend to equilibrate towards a stable value: LAI_{EHE}. Reciprocally, under given climate conditions and if LAI = LAI_{EHE}, plant RD must be sized in order to sustain the corresponding transpiration rate by accessing sufficient soil water, but not more, as otherwise, LAI_{EHE} would be larger. We further hypothesize that, as plants generally operate near their point of catastrophic xylem failure ($\Psi_{critical}$; Choat et al., 2012; Tyree & Sperry, 1988), the equilibrium RD must therefore induce a value of Ψ_{min} close to $\Psi_{critical}$, which is defined by the water potential inducing 88% and 50% loss of conductivity for angiosperms and gymnosperms, respectively (Brodribb, Bowman, Nichols, Delzon, & Burlett, 2010; Delzon & Cochard, 2014; Urli et al., 2013). Given $\Psi_{critical}$, there is a subspace of the root parameters for which $\Psi_{min} = \Psi_{critical}$. Combining the need to achieve transpiration rates imposed by LAI_{EHE} while avoiding hydraulic failure, we define the EHE-optimal RD ($Z_{optimized}$, $FRP_{optimized}$) as the point of the $\Psi_{min} = \Psi_{critical}$ subspace of the root parameters that maximizes annual transpiration (see example Figure 2a,b).

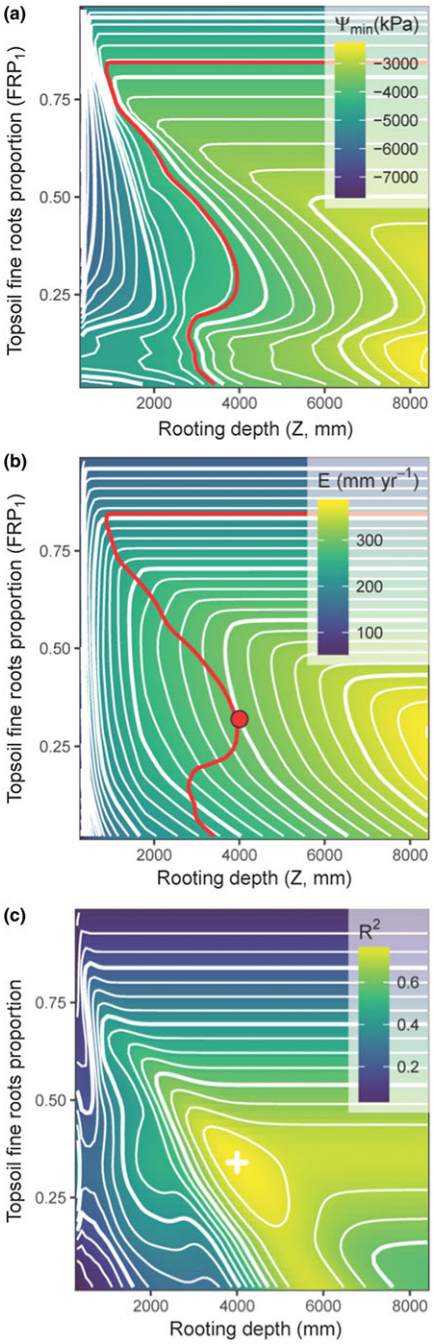

FIGURE 2 Illustration of the optimization and calibration of the root distribution parameters (rooting depth [Z], in mm; fine roots proportion in the topsoil [FRP_1]) in the case of a *Q. ilex*/*P. sylvestris* mixed stand located in the Prades Mountain. Each pixel represents a model run with a single combination of Z and FRP_1. The values taken by the response variables are represented by colour scales and white isolines: (a) *Q. ilex* minimum water potential (Ψ_{min}, in kPa). The red isoline represents the root parameters subspace where $\Psi_{min} = \Psi_{critical}$ (for *Q. ilex*, $\Psi_{critical}$ = −4,170 kPa); (b) *Q. ilex* average annual transpiration (E, in mm $year^{-1}$). The red dot represents the EHE optimum, the point of the root parameters subspace defined by a critical drought stress that maximizes E, and its coordinates correspond to the values of the optimized parameters $FRP_{1,optimized}$ and $Z_{optimized}$; (c) R^2 of the linear regression between the simulated *Q. ilex* daily transpiration and the observed one (estimated by sapflux measurements). The white cross represents the point at which R^2 is maximized ($R^2_{calibration}$ = 0.79), which corresponds to the calibrated root parameters $FRP_{1,calibrated}$ and $Z_{calibrated}$

2.8 | RD calibration and validation of RD optimization

In order to test the validity of the EHE-based optimization of RD, we used 39 experimental plots (Table 1) where sap flow or topsoil SWC was monitored. For all the plots, RD was first estimated by optimization. A second set of RD estimates was then derived by independently calibrating the model root parameters against the sap flow or topsoil SWC measurements. Although the two parameter sets, estimated by optimization and calibration, were derived independently, they are both tied to the same model and do not necessarily represent the reality due to parameters equifinality (Beven, 2006; Wang-Erlandsson et al., 2016). Consequently, the goal of this validation exercise is not to predict the real RD of vegetation but rather to assess whether the estimation of RD based on EHE optimization is suited for the parameterization of RD within water balance models.

In practice, the calibration of root parameters slightly differed depending on the type of observations. In the case of sap flow measurements, calibration consisted in running the model for each combination of Z and FRP_1 for a given range (e.g., [300–5,000 mm] and [0–1], respectively) and step (e.g., 100 mm and 0.02, respectively). For each model run, the R^2 of the linear regression between simulated and observed E was calculated. The calibrated parameters $Z_{calibrated}$ and $FRP_{1,calibrated}$ are given by the parameter combination corresponding to the maximum R^2 ($R^2_{calibration}$, represented by a white cross in the example Figure 2c). $R^2_{optimization}$ is the fit between observations and simulations obtained by parameterizing the model with the optimized RD parameters. The optimization of Z and FRP was validated by comparing $R^2_{optimization}$ to $R^2_{calibration}$ such that $R^2_{optimization} \geq 0.9 \cdot R^2_{calibration}$ (Figure 2).

As our water balance model does not account for upward water fluxes between the subsoil and the topsoil (i.e., capillary rise or hydraulic redistribution), and because $Z > Z_{topsoil}$ (i.e., 300 mm), the simulated dynamic of SWC in the topsoil is consequently independent of the SWC dynamic in the subsoil and therefore of the subsoil layer depth. Hence, when using topsoil SWC measurements, FRP_1 is the only parameter that can be calibrated. In this case, Z was set to a fixed value and the model was run for each value of FRP_1 in a given range (e.g., [0–1]) and step (e.g., 0.02). Similarly to the calibration with sap flow data, the calibrated parameter $FRP_{1,calibrated}$ was given by the FRP_1 value resulting in the maximum R^2 of the linear regression between observed and simulated daily SWC dynamics, and $R^2_{optimization}$ was obtained by parameterizing the model with $FRP_{1,optimized}$. The optimization of FRP_1 was validated by comparing $R^2_{optimization}$ to $R^2_{calibration}$ (using $R^2_{optimization} \geq 0.9 \cdot R^2_{calibration}$ as criterion). In addition, we also evaluated the linearity of the relationship between $FRP_{1,optimized}$ and $FRP_{1,calibrated}$.

2.9 | Application of the root optimization at the regional level and impact on modelled transpiration

Before producing optimized RD estimates at the regional level, we evaluated the sensitivity of plant transpiration and drought stress to RD in the context of the study area. To do so, PLC_{max} and the average annual E were simulated for all species at all the SFI3 plots in Catalonia, assuming different rooting depths (Z = 300, 500, and 1,000 mm) and a conic root architecture. We considered that a given forest plot was not water-limited if a soil depth Z = 300 mm was enough to obtain PLC_{max} < 50%.

The optimized RD of the water-limited SFI3 plots (approximately 5,000 plots, Figure S3B) was then calculated, using meteorological data of the period 1999–2001 or 2000–2002 in order to encompass the year when SFI3 plots were surveyed (2000 and 2001). In order to evaluate the benefits of optimizing plant RD at the regional scale, we compared the transpiration simulated using optimized RD (set at the plot level as the optimized RD of the dominant species) with the transpiration obtained assuming constant values of Z (500 or 1,000 mm; cf. De Cáceres et al., 2015; Nadal-Sala, Sabaté, & Gracia, 2013) and a conic RD.

To analyse the factors driving the regional variations of optimized RD estimates, we fitted general linear models for both $Z_{optimized}$ and $FRP_{1,optimized}$, using environmental variables and species parameters as explanatory variables. The explanatory variables used for each model was a subset of an initial selection of water balance inputs (mean annual and summer values for precipitation, temperature, and potential evapotranspiration, stand LAI, RFC, $\Psi_{critical}$ and $\Psi_{extract}$), as well as their interactions. The final variables were selected using type I analysis of variance and setting a minimum significance α = 0.0001.

3 | RESULTS

3.1 | Effect of water-limitation on the sensitivity of modelled transpiration to RD

Simulated E strongly varied across SFI3 plots over the period 1999–2002 (Figure 3). The lowest E values correspond to plots with low LAI (e.g., those recovering from recent wild fires). Plots were classified according to the minimum rooting depth (Z_{min}) inducing PLC_{max} < 50% (i.e., moderate drought stress), which can be assimilated to a soil water-reliance criterion. For the plots that were not limited by soil water (i.e., Z_{min} < 300 mm), simulated E was only slightly affected by rooting depth. On the contrary, water-limited plots (i.e., Z_{min} > 300 mm) exhibited a highly significant increase of simulated E with rooting depth, the increase being larger for more water-limited plots.

3.2 | Validation of the RD optimization using sap flow measurements

E and Ψ_{min} were simulated for *Q. ilex* and *P. sylvestris* for about 2,500 combinations of Z (300–8,000 mm) and FRP_1 (0–1) at the three plots in the Prades Mountains where sap flow was measured in 2010 and 2011. Similarly to the case of *Q. ilex* in mixed stand (Figure 2; see Figures S1 and S2 for details on the three other cases), in the general case, E monotonically increased with Z although the increase was very small for FRP_1 values close to 1 (i.e., very shallow root system). For a given Z, E was maximized for a FRP_1 value that was generally comprised between 0.25 and 0.75 and that decreased with increasing Z. Ψ_{min} varied with Z and FRP1 in a more complex way than E (see Figure 2 for a representative example) but was generally more

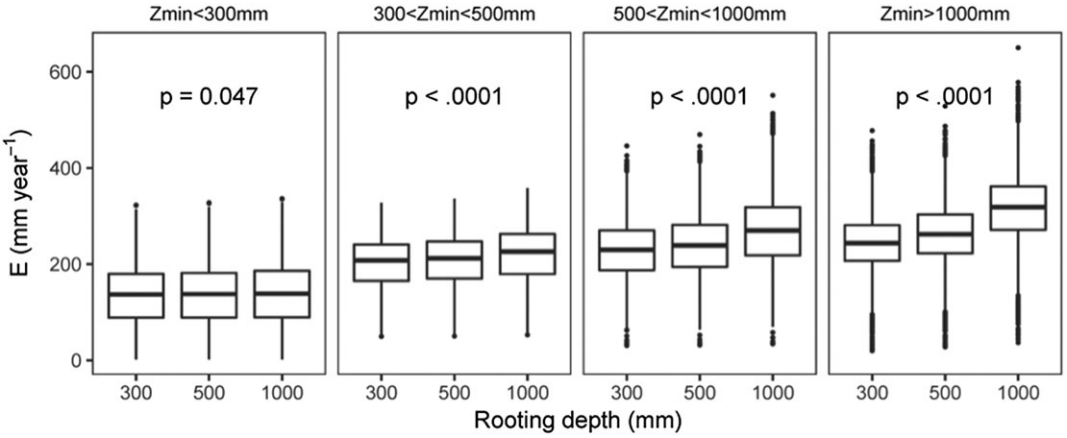

FIGURE 3 Average annual transpiration (*E*) simulated for the SFI3 plots in Catalonia on the period 1999–2002, given three different rooting depths and assuming a conic root architecture. Plots are split into different panels according to the minimum rooting depth (Z_{min}) for which PLC_{max} < 50%, as indicated at the top of each panel. The *p* values of transpiration differences between rooting depths were calculated within each panel using one-way analysis of variance

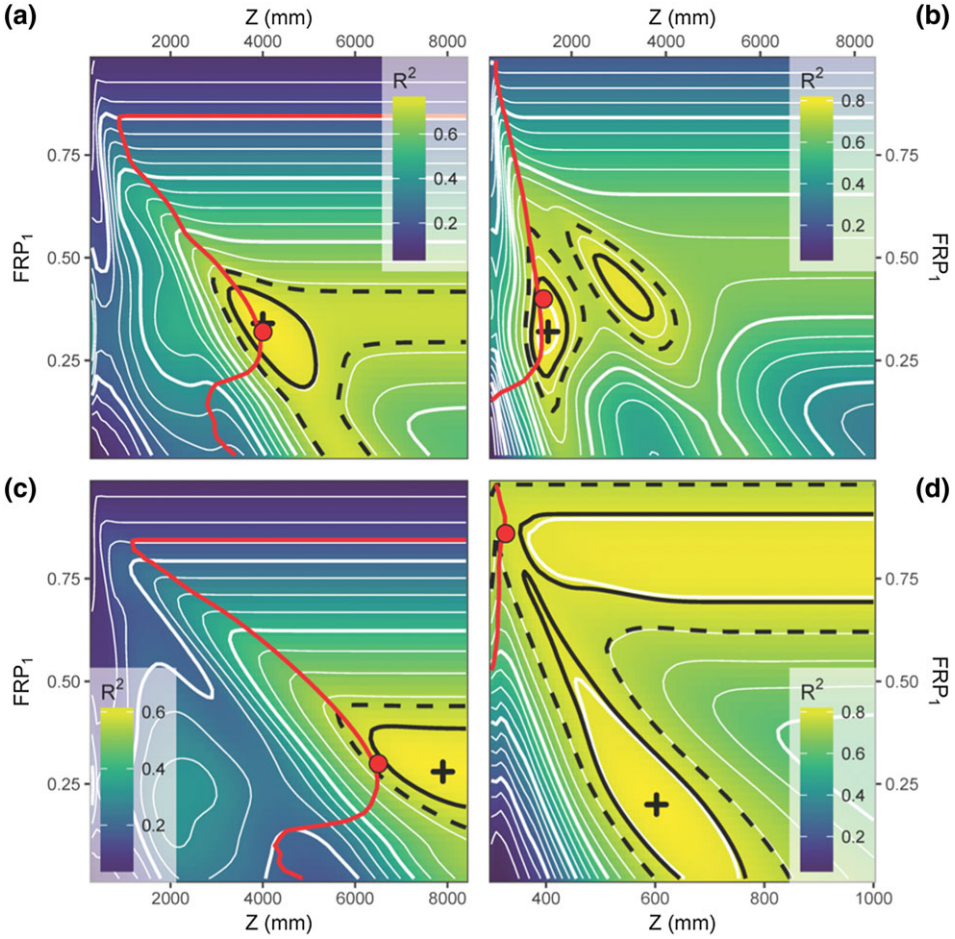

FIGURE 4 Graphical output of the root parameters (rooting depth [Z], in mm; fine roots proportion in the topsoil [FRP_1]) optimization and calibration process using sap flow measured on two species at three different plots located in the Prades Mountains: (a) *Q. ilex*, mixed stand; (b) *P. sylvestris*, mixed stand; (c) *Q. ilex*, pure stand; and (d) *P. sylvestris*, pure stand. The colour gradient and white contour lines represent the R^2 of the regression between measured and simulated daily transpiration. The black cross represents the point where R^2 is maximized, whereas the black solid lines delimit the area where $R^2(Z, FRP_1) \geq 0.95 \cdot R^2_{calibration}$ and the black dashed lines delimit the area where $R^2(Z, FRP_1) \geq 0.90 \cdot R^2_{calibration}$. $R^2_{calibration}$ = 0.79, 0.81, 0.63, and 0.84 for (a), (b), (c), and (d), respectively. The red line represents the combinations of *Z* and FRP_1 for which $\Psi_{min} = \Psi_{critical}$ and the red dot is the point of this line that maximizes *E* (i.e., the EHE-optimum solution). Note the scale difference in the *x*-axis of (d)

negative for shallower RDs (i.e., smaller Z and/or higher FRP_1). Because there was a strong interactive effect between Z and FRP_1 on Ψ_{min}, the isoline $\Psi_{min} = \Psi_{critical}$ was highly non-linear. However, the Ψ isoline tended to follow a general pattern with a trend towards deeper Z values for intermediate FRP_1. That portion of the Ψ isoline also corresponded to higher E values and therefore contained the EHE-optimum solution. Notably, the optimum RD was deeper for oaks (Figure 4a,c, $Z_{optimized}$ = 4,000 and 6,500 mm) than pines (Figure 4b,d, $Z_{optimized}$ = 1,400 and 326 mm).

The R^2 of the linear regression between predicted and measured E was highly dependent on Z and FRP_1 and ranged between 0.002 and 0.84 (Figure 4). The areas for which R^2 is close to its maximum ($R^2 > 0.90 \cdot R^2_{calibration}$) can be interpreted as the uncertainty of the parameter estimates given by calibration. The uncertainty surrounding the calibrated RD estimates was therefore rather small, except in the case of the pure pine stand. The solution given by optimization was really close to the calibration estimates of the RD parameters in the case of the mixed stand, for oak and pine. The optimization estimates were however shallower than the calibration estimates in the case of the pure oak and pure pine stands, $Z_{optimized}$ being inferior to $Z_{calibrated}$ by nearly 2,000 mm in the case of the pure oak stand (Figure 4c). The optimization estimates nevertheless always fell within the space delimited by $R^2 > 0.9 \cdot R^2_{calibration}$.

3.3 | Validation of the topsoil root proportion optimization using soil moisture measurements across a canopy density gradient

FRP_1 was estimated by calibration and optimization for 27 out of 28 *P. pinaster* plots located in the Prades Mountain where SWC was measured (Figure 5a–c). One plot was discarded because of the absence of a clear calibration solution (low R^2 values and little variations in response to changes in FRP_1). FRP_1 as estimated both by calibration and optimization was closely related to the stand LAI and RFC (Figure 5a,b; R^2 = 0.80 and 0.78, respectively), with FRP_1 being predicted to decrease for increasing values of LAI or RFC. However, calibration estimates were more sensitive to LAI and RFC than the optimization estimates, as shown by the slopes of the fitted regression models (Figure 5a,b). As a result, calibration and optimization estimates were also well correlated to each other (Figure 5c, R^2 = 0.78) but $FRP_{1,calibrated}$ varied over a wider range than $FRP_{1,opitmized}$,

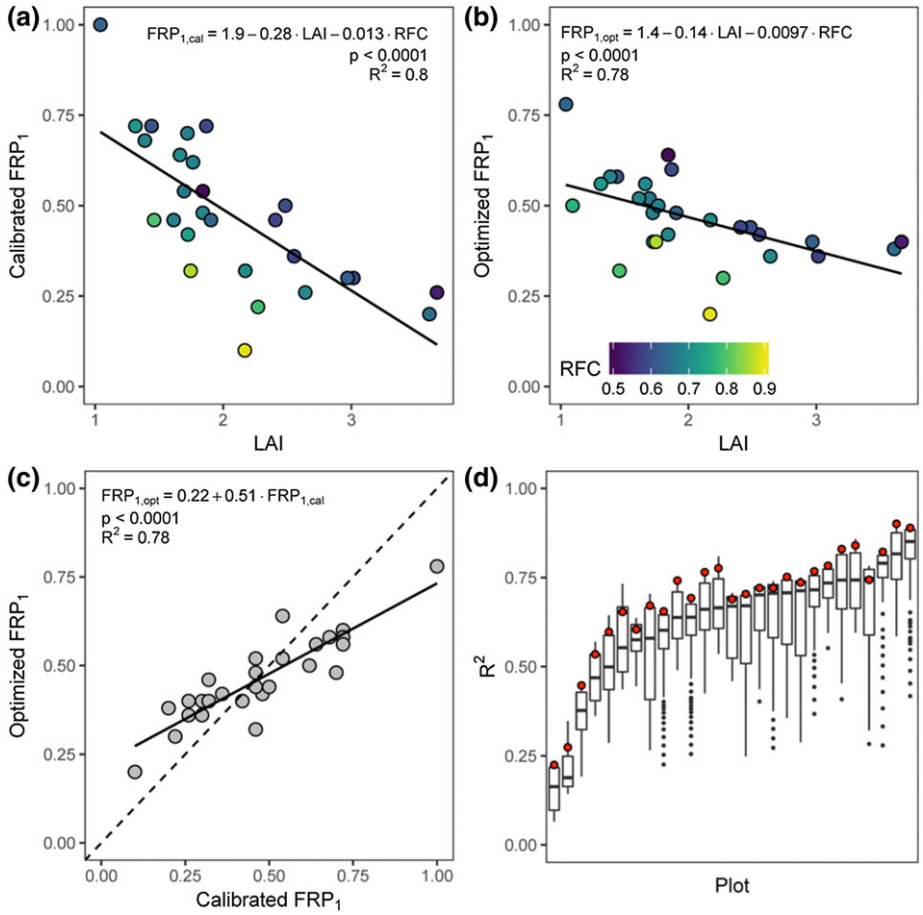

FIGURE 5 Topsoil root proportion (FRP_1) estimated by calibration (a) and optimization (b) for 27 *P. pinaster* plots located in the Prades Mountain, as a function of the stand leaf area index (LAI) and the soil rock fragment content (RFC). The solid lines represent the linear regressions between FRP_1 and LAI. The multiple linear regressions, including the effect of both LAI and RFC raised (a) R^2 = 0.80 and (b) R^2 = 0.78. (c) Correlation between the estimates of the root proportion in the topsoil (FRP_1) obtained by calibration and optimization (R^2 = 0.78). (d) Boxplot of the goodness of the fit (R^2) between measured soil water content and the output of 100 simulations per plot with FRP_1 ranging between 0.01 and 1. Plots are ranked by median R^2 value. The red dots indicate the R^2 when $FRP_1 = FRP_{1,optimized}$ (i.e., $R^2_{optimization}$). Note that $R^2_{optimization}$ is generally close to the maximum R^2 value (i.e., $R^2_{calibration}$)

resulting in the slope of the regression significantly differing from one (slope = 0.51 ± 0.05).

When parameterized with $FRP_{1,calibrated}$, the soil water balance model globally performed well to simulate SWC dynamics in most of the plots (Figure 5d, $R^2_{calibration} > 0.6$ in 22 out of 27 plots). The model proved sensitive to FRP_1, as the R^2 range was 0.35 on average for FRP_1 values varying between 0.01 and 1, although the magnitude of this effect was plot-dependent. Using $FRP_{1,optimized}$ to parameterize the model generally raised R^2 values ($R^2_{optimization}$) close to $R^2_{calibration}$: 22 plots out of 27 fulfilled the criterion $R^2_{optimization} > 0.90 \cdot R^2_{calibration}$.

3.4 | Effect of water-limitation on RD optimization

The FRP_1 estimates derived by calibration and optimization of the water balance model at the eight *P. sylvestris* plots with soil moisture measurements were not significantly correlated (Figure 6a, $p = 0.09$, adjusted $R^2 = 0.30$). Overall, the optimization resulted in a large overestimation of FRP_1 relatively to calibration. However, the absolute difference between the two estimates was largely explained by the ratio between LAI and summer precipitations ($p < 0.005$, adjusted $R^2 = 0.78$), a proxy of stand water limitation (under given precipitations, a higher LAI implies a reduction in stand water availability). $FRP_{1,optimized}$ was therefore closer to $FRP_{1,calibrated}$ for the plots with a relatively high LAI and/or located at the drier end of the climatic gradient.

3.5 | Optimization of RD at the regional scale (Catalonia)

Overall, 95% of optimized *Z* estimates of the approximately 5,000 water-limited SFI3 plots are comprised between 320 and 4,000 mm, with a median value of 700 mm. Variations in $Z_{optimized}$ were explained by climatic (log P_{summer} and PET_{summer}), edaphic (RFC), structural (LAI), and species hydraulics ($\Psi_{critical}$ and $\Psi_{extract}$) factors ($R^2 = 0.59$, $p < 0.0001$; Table 2).

The optimum RD was found to be deeper for plots with dryer climate, rockier soil, and higher LAI (Table 2). Deeper RD was also predicted for species that were more vulnerable to embolism (lower

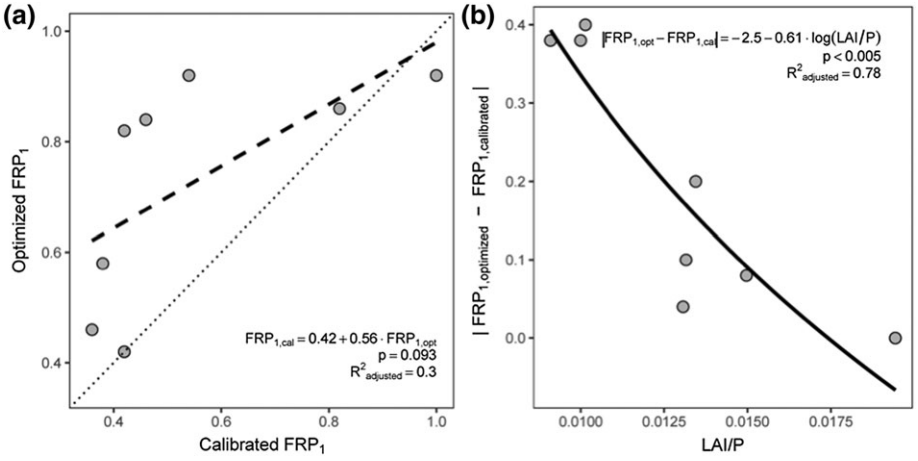

FIGURE 6 (a) Relationship between optimization and calibration estimates of topsoil root proportion (FRP_1) for eight *P. sylvestris* plots located along the climatic gradient occupied by the species in Catalonia. The correlation between the two estimates is not significant ($p = 0.093$). (b) The absolute difference between the optimization and calibration estimates is correlated to the logarithm of the ratio between leaf area index (LAI) and average summer precipitation (P) ($p < 0.005$, adjusted $R^2 = 0.78$)

TABLE 2 Summary of the linear models used to quantify the role of the different climatic, edaphic, structural, and hydraulic variables on the optimized values of *Z* and FRP_1

		log $Z_{optimized}$		$FRP_{1,optimized}$	
	Effect	Standardized coefficients	Sum of squares (type I ANOVA)	Standardized coefficients	Sum of squares (type I ANOVA)
Main	log $Z_{optimized}$			−0.87	8,012
	LAI	0.80	1,833	0.29	993
	log P_{summer}	−0.40	1,200		
	$\lvert\Psi_{critical}\rvert$	−0.25	384	−0.26	345
	$\lvert\Psi_{extract}\rvert$	0.47	930	0.11	25
	RFC	0.45	2,001		
	PET_{summer}	0.20	420		
Interactions	LAI: log P_{summer}	−0.17	468		
	LAI: $\lvert\Psi_{critical}\rvert$	−0.41	204		
	LAI: $\lvert\Psi_{extract}\rvert$	0.32	320		
	Full model		7,760		9,375
	Residuals		5,401		3,788

Note. Both models could explain most of the variance of the optimized root distribution ($R^2 = 0.59$ and $R^2 = 0.71$ for $Z_{optitmized}$ and $FRP_{1,optimized}$, respectively). Models were fitted on standardized variables. Sums of squares were estimated with type I ANOVA. All included effects were strongly significant ($p < 0.0001$). ANOVA: Analysis of variance; FRP: fine root proportion; LAI: leaf area index; PET: potential evapotranspiration; RFC: rock fragment content.

$|\Psi_{critical}|$) and had a less sensitive transpiration to declining soil water availability (higher $|\Psi_{extract}|$). The negative interaction between LAI and summer precipitation caused the sensitivity of $Z_{optimized}$ to LAI to be stronger for low precipitation areas and conversely, the sensitivity of $Z_{optimized}$ to precipitation to be stronger for higher LAI values (see Figure S5A for graphical visualization of the interaction). Similarly, the sensitivity of $Z_{optimized}$ to LAI was positively related to $|\Psi_{extract}|$ (Figure S5B) and negatively to $|\Psi_{critical}|$ (Figure S5C).

About 95% of the optimized topsoil root proportion values were comprised between 0.18 and 0.92, the median value being 0.6. Variations in $FRP_{1,optimized}$ were mostly explained by the variations of the corresponding optimum rooting depth (Table 2). The main factors that had an effect on $FRP_{1,optimized}$ besides $Z_{optimized}$ were the stand LAI and the species hydraulic parameters $|\Psi_{critical}|$ and $|\Psi_{extract}|$: For a given $Z_{optimized}$, the optimum topsoil root proportion increased with LAI and $|\Psi_{extract}|$ and decreased with $|\Psi_{critical}|$.

3.6 | Effect of RD optimization on modelled transpiration

When using the optimum RD to parameterize the water balance model, 95% of plot transpiration ranged between 127 and 467 mm $year^{-1}$ (Figure 8a) and was 284 mm $year^{-1}$ on average. Using alternative parameterizations with fixed Z values of 500 and 1,000 mm, which corresponds to sound average soil depth estimates, and assuming a conic root architecture had a strong effect on the simulated E (Figure 8b). The average E difference relative to simulations with optimized RD estimates (ΔE) was of −14% for Z = 500 mm and ranged between −29% and −1% (5th and 95th percentiles). When Z was set to 1,000 mm, resulting simulated E was on average similar to E simulated using the optimized root parameters, but ΔE for individual plots ranged between −13% and 13% (5th and 95th percentiles). For Z = 500 mm, ΔE was more negative for the forests of the coastal fringe (Figure 8c), whereas for Z = 1,000 mm, the deviation was stronger and positive for the forests of central-northern Catalonia (Figure 8d).

4 | DISCUSSION

4.1 | RD heterogeneity and water balance modelling in water-limited forest

Remarkable variations in RD (and especially rooting depth) have been reported at different scales, from broad patterns across biomes and life forms (Canadell et al., 1996; Fan et al., 2017; Jackson et al., 1996; Schenk & Jackson, 2002a; Schulze et al., 1996) to differences between genera and species (Fan et al., 2017; Hamer et al., 2016; Stone & Kalisz, 1991) and even within species (Kirchen et al., 2017; López, Sabaté, & Gracia, 1998; Schmid & Kazda, 2002; Sperry, Hacke, Oren, & Comstock, 2002). Accordingly, the EHE-based optimization predicted RD to vary greatly both among stands and between species (Figure 7). Our results show that these variations have a strong effect on the water balance of forest stands by determining the amount of stored soil water that plants have access to (Figure 8). Assuming the rooting depth to be constant led to important overestimation or underestimation of modelled transpiration in some areas, compared with estimates derived from the EHE optimization. Furthermore, the simulation deviations were expressed in terms of total annual transpiration, but they are likely to be greater for summer, when vegetation critically relies on soil water reserves. Therefore, properly estimating vegetation rooting depth is essential for quantifying water fluxes through the soil–plant-atmosphere continuum (Bleby, Mcelrone, & Jackson, 2010; Granier et al., 2007; Zeng et al., 1998) and predicting vegetation dynamic processes such as drought-induced die-off events, which are expected to increase under climate change (Allen et al., 2010; Allen, Breshears, & McDowell, 2015; Anderegg et al., 2013; McDowell et al., 2011, 2013).

4.2 | Applying the EHE hypothesis to predict RD in water-limited forests

Optimum RD was generally consistent with the RD as estimated by independent calibration of the root parameters, and both estimates performed similarly in the context of our water balance model (e.g.,

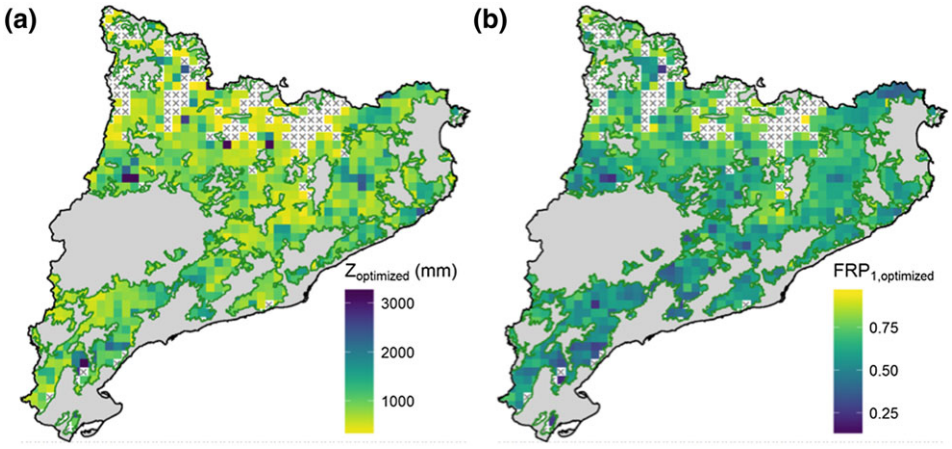

FIGURE 7 Map of the optimized root parameters Z (a) and FRP^1 (b) of the approximately water-limited 5,000 SFI3 plots located in Catalonia. Values are averages of optimized parameters for dominant species of the plots located within the area of each 5 × 5 km^2 pixel. Empty pixels (caused by a lack of data or nonwater limiting conditions for the plots within the pixel area) are represented by the symbol "×." Most nonwater limited plots are located in the north of the territory, in the Pyrenean Mountain range. Grey areas indicate nonforested regions

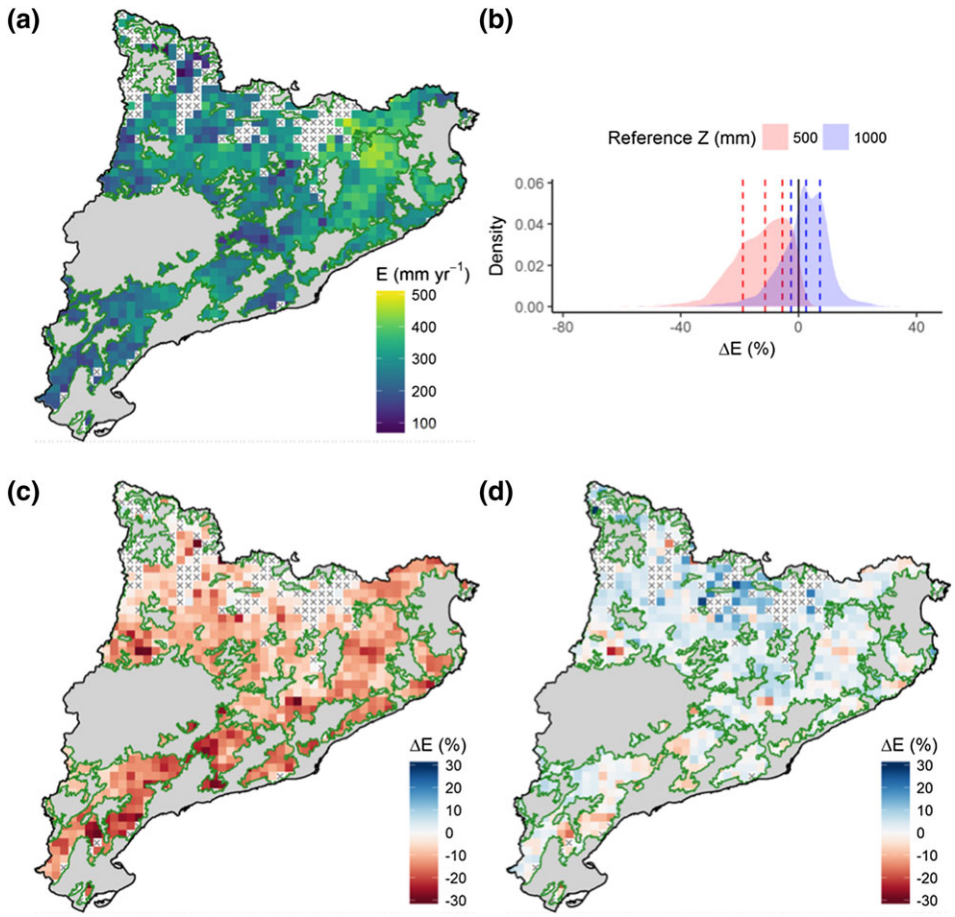

FIGURE 8 (a) SFI3 plots annual transpiration (E) for the period 1999–2002 simulated by using the optimized root distribution (RD). (b) Density distribution of the plots value of the transpiration relative change induced by parameterizing Z to fixed values (500 or 1,000 mm), compared with the transpiration simulated with the optimum RD (ΔE, defined as $(E_Z - E_{optimized})/E_{optimized}$). Dashed lines represent the first, second, and third quartiles. (c) ΔE for Z = 500 mm. (d) ΔE for Z = 1,000 mm. In (a), (c), and (d), plots values are spatially averaged within the area of each 5 × 5 km^2 pixel. Empty pixels (caused by a lack of data or nonwater limiting conditions for the plots within the pixel area) are represented by the symbol "×." Grey areas indicate nonforested regions

Figure 5c,d). Because it allowed the calibration of both RD parameters Z and FRP, the use of sap flow data to validate the optimization of RD (Figure 4) was more powerful than using soil moisture data, which nevertheless compensated for the lower number of sap flow series. Although the optimization of RD was successful to retrieve the calibrated root parameters, the optimum RD does not necessarily represent the real RD but rather a model-wise estimation of RD given a specific model formulation (parameters equifinality, Beven, 2006).

The optimization of RD nevertheless reproduced many expected patterns in response to climate, soil, and vegetation structure (Table 2). The optimized rooting depth was strongly and positively related to the stand LAI (Figure 5b, Table 2), which is a consequence of the EHE assuming that, other variables being equal, a higher LAI implies an enhanced transpiration rate (Granier et al., 1999) and thus the need to balance the higher water demand by accessing additional water resources. This does not mean that higher LAI causes roots to be deeper but, on the contrary, that deeper roots increase the amount of water available to vegetation, which in turn allows the vegetation to sustain a higher LAI (Grier & Running, 1977; Nemani & Running, 1989). Similarly, soils with a higher proportion of rock content induced deeper optimum root system to compensate for the loss of water holding capacity per unit of soil volume. This result is in agreement with the observation of Kirchen et al. (2017) that the root system of a homogeneous beech stand in NE France clearly responded to sequential reductions in soil water holding capacity by increasing the proportion of roots in the deepest horizons.

4.3 | Stand water balance drives the optimum RD through plant hydraulics

The optimization of RD according to the EHE led to assume water availability to be a primary shaping factor of RD, which is sustained by results from intensive sampling at the global scale (Schenk & Jackson, 2002a, 2002b). The EHE hypothesis also predicts that the depth of RD should increase with water scarcity, which is consistent with previous reports (Schenk & Jackson, 2002a; Schulze et al., 1996). Besides substantiating this prediction, in this study, we found that factors such as LAI and RFC also have a large effect on RD, therefore highlighting the importance of taking into account the whole water balance of a stand to understand RD variations instead of relying solely on climatic factors.

Although no assumption was made on root architecture when optimizing RD, the resulting Z and FRP_1 exhibited a strong correlation, suggesting that, to a certain extent, the shape of the optimum root

profile is conserved across environmental conditions. Furthermore, even for deep-rooted plants, most of the roots were located in the topsoil. This is consistent with the global pattern of exponentially declining fine root density with increasing depth (Jackson et al., 1996; Schenk, 2008). It also agrees with the principle of the shallowest possible water extraction profile formulated by Laio, D'Odorico, and Ridolfi (2006) and Schenk (2008); according to which, RD must be as shallow as possible due to the patterns of water infiltration and nutrient distribution, the availability of which generally decreases with depth (Jobbágy & Jackson, 2001). In our modelling framework, however, the optimized root profile may not always match the water infiltration profile as SWC is initialized at field capacity, which potentially induces an overestimation of soil moisture in the subsoil, at least at the beginning of each simulation. Nonetheless, this assumption appears reasonable as simulations started during winter months, and in the study area, autumn and spring are the two wettest seasons (Ninyerola et al., 2000), and transpiration is low during winter (data not shown).

In our study, 2% of optimized cohorts were simulated to access a water holding capacity larger than the annual precipitations. This inconsistency may be due to some discrepancies in the parameterization of the water balance model (e.g., too high LAI relative to precipitation). Alternatively, it might be an indication that plants at these locations do not solely rely on precipitation but are also able to tap groundwater. Groundwater was previously shown to be an important source of water for ecosystems under certain conditions (Condon & Maxwell, 2017; Maxwell & Condon, 2016) and can help vegetation to maintain higher LAI under dry climates (Smettem, Waring, Callow, Wilson, & Mu, 2013). Owing to the extensive presence of shallow soils over deep groundwater reserves in Mediterranean ecosystems, groundwater is indeed likely to be an important source of water in our study area (Barbeta et al., 2015; Llorens et al., 2010; Nardini et al., 2016; Witty, Graham, Hubbert, Doolittle, & Wald, 2003).

Species with different hydraulic strategies are expected to have contrasting RDs (Sperry & Hacke, 2002). In our study, we found rooting depth to vary in relation with the hydraulic parameters $\Psi_{extract}$ and $\Psi_{critical}$, which represent the sensitivity of the whole plant conductance to drying soil and the plant ability to resist low water potentials, respectively. More negative $\Psi_{extract}$ values allowed plants to maintain transpiration rates at more negative water potentials. As a consequence, Ψ_{plant} declined faster, which caused the optimum RD to be deeper for those species. This result is in agreement with the observations that deep-rooted species are generally able to maintain transpiration for longer during dry periods (Meinzer et al., 2013; Sperry & Hacke, 2002). This result is also consistent with the somewhat paradoxical observation that deep-rooted species can reach more negative water potentials during the growing season (Pivovaroff et al., 2016). On the other hand, $\Psi_{critical}$ controlled the yearly minimum water potential that vegetation reached on average. Our model predicted that species with a more negative $\Psi_{critical}$ have a shallower optimum RD, which is consistent with the positive relationship between rooting depth and hydraulic vulnerability reported for tropical moist forests (Lopez, Kursar, Cochard, & Tyree, 2005) as well as in hot (Hacke, Sperry, & Pittermann, 2000; Sperry & Hacke, 2002) and cold deserts (Bucci et al., 2009, 2013). As a result, the differences in species hydraulic parameters used in the model led to a clearly shallower distribution for pines than oaks, mimicking the known rooting habits of these two genera (Abrams, Schultz, & Kleiner, 1990; del Castillo, Comas, Voltas, & Ferrio, 2016; Meinzer et al., 2013; Oren & Pataki, 2001).

4.4 | Limitations and generalization

The optimization of RD by maximizing *E* while constraining the plant water potential such that $\Psi_{min} = \Psi_{critical}$ entails the hypothesis that the vegetation operates near its point of catastrophic xylem failure (Tyree & Sperry, 1988), regardless of the environmental conditions. Although this assumption appeared realistic for water-limited plots, it failed to predict FRP_1 for the *P. sylvestris* stands with higher water availability. Generally, the agreement between optimization and calibration estimates of RD increased with drier conditions. This suggests that vegetation may deviate from the EHE as water becomes less limiting, as it was proposed in Eagleson's original theory (Eagleson, 1982). However, the high plasticity of plant traits such as cavitation resistance (Anderegg, 2015; Bryukhanova & Fonti, 2013; Wortemann et al., 2011) or hydraulic architecture (DeLucia, Maherali, & Carey, 2000; Limousin et al., 2012; Martínez-Vilalta et al., 2009) allows plants to hydraulically adjust to their environment. Furthermore, taking into account the carbon economy to estimate the cost of root construction and maintenance could improve RD estimates, particularly when water is less limiting.

When there were several species per plot, each species' RD was optimized by assimilating interspecific competition to intraspecific competition, that is, assuming no species-specific interactions. This strong assumption led to consistent results in the case of the mixed *P. sylvestris* and *Q. ilex* stand, the only validation plot that included more than one species. These two species belong to genera known to have contrasting rooting habits (Abrams, 1990; Abrams et al., 1990; del Castillo et al., 2016; Meinzer et al., 2013; Oren & Pataki, 2001) that were retrieved in our estimations. It is possible that in the case of species sharing more similar potential RDs, competition would actually induce a vertical partitioning of the root system between species (Schmid & Kazda, 2002).

In this work, the optimization of RD is based on the maximization of transpiration and the restriction of plant drought stress. This method could thus be applied to any water balance model that simulates both plant transpiration and drought stress. Although only two soil layers were considered here, setting to two the number of parameters to optimize, the RD optimization could be generalized to a greater number of soil layers by using an architectural model, such as the LDR model proposed by Schenk and Jackson (2002a), in order to limit the dimensions of the root parameter space. Increasing the number of soil layers represented in a model can substantially improve the modelling of water fluxes (Guswa, Celia, & Rodriguez-Iturbe, 2004) by better taking into account vertical heterogeneity, which is crucial for the representation of underground competition.

5 | CONCLUSIONS

The use of a robust description of drought stress based on plant hydraulics together with the concept of EHE proved successful to

derive estimates of RD that were meaningful in the context of our model and that largely reproduced expected relationships between climate, soil, canopy density, species hydraulic traits, and RD. The application of optimization to derive RD estimates failed when water was not limiting, but under these conditions, vegetation relies less on soil water storage, and the sensitivity of modelled transpiration to RD is low. The uncertainty regarding root parameters should therefore not blur vegetation dynamics predictions in this case. This work is a step towards an ecologically sound RD parameterization of vegetation models at large spatial scales, which is crucial for modelling water and carbon fluxes and anticipating the effect of climate change on vegetation dynamics. The optimization of RD could be further improved by integrating a more realistic description of plant's hydraulic behaviour (cf. Sperry et al., 2016), as well as by taking advantage of the increased availability of spatially resolved trait data to better represent intraspecific and interspecific variations in hydraulic traits and architecture.

ACKNOWLEDGEMENTS

This research was supported by the Spanish Ministry of Economy and Competitiveness through projects FORESTCAST (CGL2014-59742-C2-2-R), FUN2FUN (CGL2013-46808-R), SAPFLUXNET (CGL2014-5583-JIN), and MYCOSYSTEMS (AGL2015-66001-C3-1-R), an FPI predoctoral contract to A. C. (BES- 2015-071350) and a "Ramon y Cajal" fellowship to M. D. C. (RYC-2012-11109). J. M. V. benefited from an ICREA Academia award. The authors want to thank the "Agencia Estatal de Meteorología" (AEMET) and "Servei Meteorològic de Catalunya" (SMC) for providing daily weather station data.

ORCID

Antoine Cabon http://orcid.org/0000-0001-6426-1726

REFERENCES

Abrams, M. D. (1990). Adaptations and responses to drought in Quercus species of North America. *Tree Physiology*, *7*, 227–238. https://doi.org/10.1093/treephys/7.1-2-3-4.227

Abrams, M. D., Schultz, J. C., & Kleiner, K. W. (1990). Ecophysiological responses in mesic versus xeric hardwood species to an early-season drought in central Pennsylvania. *Forest Science*.

Adams, H. D., Zeppel, M. J. B., Anderegg, W. R. L., Hartmann, H., Landhäusser, S. M., Tissue, D. T., … McDowell, N. G. (2017). A multi-species synthesis of physiological mechanisms in drought-induced tree mortality. *Nature Ecology and Evolution*, *1*, 1285–1291. https://doi.org/10.1038/s41559-017-0248-x

Aguadé, D., Poyatos, R., Rosas, T., & Martínez-Vilalta, J. (2015). Comparative drought responses of Quercus ilex L. and Pinus sylvestris L. In a montane forest undergoing a vegetation shift. *Forests*, *6*, 2505–2529. https://doi.org/10.3390/f6082505

Allen, C.D., Breshears, D.D., McDowell, N.G., 2015. On underestimation of global vulnerability to tree mortality and forest die-off from hotter drought in the Anthropocene. *Ecosphere 6*, art129. https://doi.org/10.1890/ES15-00203.1

Allen, C. D., Macalady, A. K., Chenchouni, H., Bachelet, D., McDowell, N., Vennetier, M., … Cobb, N. (2010). A global overview of drought and heat-induced tree mortality reveals emerging climate change risks for forests. *Forest Ecology and Management*, *259*, 660–684. https://doi.org/10.1016/j.foreco.2009.09.001

Anderegg, L. D. L., Anderegg, W. R. L., & Berry, J. A. (2013). Not all droughts are created equal: Translating meteorological drought into woody plant mortality. *Tree Physiology*, *33*, 701–712. https://doi.org/10.1093/treephys/tpt044

Anderegg, W. R. L. (2015). Spatial and temporal variation in plant hydraulic traits and their relevance for climate change impacts on vegetation. *The New Phytologist*, *205*, 1008–1014. https://doi.org/10.1111/nph.12907

Anderegg, W. R. L., Klein, T., Bartlett, M., Sack, L., Pellegrini, A. F. A., Choat, B., & Jansen, S. (2016). Meta-analysis reveals that hydraulic traits explain cross-species patterns of drought-induced tree mortality across the globe. *Proceedings of the National Academy of Sciences*, *113*, 5024–5029. https://doi.org/10.1073/pnas.1525678113

Andreu, L., Gutiérrez, E., Macias, M., Ribas, M., Bosch, O., Camarero, J.J., 2007. Climate increases regional tree-growth variability in Iberian pine forests. *Global Change Biology 16*, 070228013259001–???. https://doi.org/10.1111/j.1365-2486.2007.01322.x

Balandier, P., Marquier, A., Casella, E., Kiewitt, A., Coll, L., Wehrlen, L., & Harmer, R. (2013). Architecture, cover and light interception by bramble (Rubus fruticosus): A common understorey weed in temperate forests. *Forestry*, *86*, 39–46. https://doi.org/10.1093/forestry/cps066

Barbeta, A., Mejía-Chang, M., Ogaya, R., Voltas, J., Dawson, T. E., & Peñuelas, J. (2015). The combined effects of a long-term experimental drought and an extreme drought on the use of plant-water sources in a Mediterranean forest. *Global Change Biology*, *21*, 1213–1225. https://doi.org/10.1111/gcb.12785

Beven, K. (2006). A manifesto for the equifinality thesis. *Journal of Hydrology*, *320*, 18–36. https://doi.org/10.1016/j.jhydrol.2005.07.007

Bleby, T. M., Mcelrone, A. J., & Jackson, R. B. (2010). Water uptake and hydraulic redistribution across large woody root systems to 20 m depth. *Plant, Cell and Environment*, *33*, 2132–2148. https://doi.org/10.1111/j.1365-3040.2010.02212.x

Bonet, J. A., De-Miguel, S., Martínez de Aragón, J., Pukkala, T., & Palahí, M. (2012). Immediate effect of thinning on the yield of Lactarius group deliciosus in Pinus pinaster forests in Northeastern Spain. *Forest Ecology and Management*, *265*, 211–217. https://doi.org/10.1016/j.foreco.2011.10.039

Bréda, N., Granier, A., & Aussenac, G. (1995). Effects of thinning on soil and tree water relations, transpiration and growth in an oak forest (Quercus petraea (Matt.) Liebl.). *Tree Physiology*, *15*, 295–306. https://doi.org/10.1093/treephys/15.5.295

Brienen, R. J. W., & Zuidema, P. A. (2005). Relating tree growth to rainfall in Bolivian rain forests: A test for six species using tree ring analysis. *Oecologia*, *146*, 1–12. https://doi.org/10.1007/s00442-005-0160-y

Brodribb, T., & Hill, R. S. (1999). The importance of xylem constraints in the distribution of conifer species. *The New Phytologist*, *143*, 365–372. https://doi.org/10.1046/j.1469-8137.1999.00446.x

Brodribb, T. J. (2017). Progressing from 'functional' to mechanistic traits. *The New Phytologist*, *215*, 9–11. https://doi.org/10.1111/nph.14620

Brodribb, T. J., Bowman, D. J. M. S., Nichols, S., Delzon, S., & Burlett, R. (2010). Xylem function and growth rate interact to determine recovery rates after exposure to extreme water deficit. *The New Phytologist*, *188*, 533–542. https://doi.org/10.1111/j.1469-8137.2010.03393.x

Bryukhanova, M., & Fonti, P. (2013). Xylem plasticity allows rapid hydraulic adjustment to annual climatic variability. *Trees - Structure and Function*, *27*, 485–496. https://doi.org/10.1007/s00468-012-0802-8

Bucci, S. J., Scholz, F. G., Goldstein, G., Meinzer, F. C., & Arce, M. E. (2009). Soil water availability and rooting depth as determinants of hydraulic architecture of Patagonian woody species. *Oecologia*, *160*, 631–641. https://doi.org/10.1007/s00442-009-1331-z

Bucci, S. J., Scholz, F. G., Peschiutta, M. L., Arias, N. S., Meinzer, F. C., & Goldstein, G. (2013). The stem xylem of Patagonian shrubs operates far from the point of catastrophic dysfunction and is additionally protected from drought-induced embolism by leaves and roots. *Plant, Cell and Environment*, *36*, 2163–2174. https://doi.org/10.1111/pce.12126

Canadell, J., Jackson, R., Ehleringer, J., Mooney, H. A., Sala, O. E., & Schulze, E.-D. (1996). Maximum rooting depth of vegetation types at the global scale. *Oecologia*, *108*, 583–595. https://doi.org/10.1007/BF00329030

Caylor, K. K., Scanlon, T. M., & Rodriguez-Iturbe, I. (2009). Ecohydrological optimization of pattern and processes in water-limited ecosystems: A trade-off-based hypothesis. *Water Resources Research*, *45*, 1–15. https://doi.org/10.1029/2008WR007230

Choat, B., Jansen, S., Brodribb, T. J., Cochard, H., Delzon, S., Bhaskar, R., … Zanne, A. E. (2012). Global convergence in the vulnerability of forests to drought. *Nature*, *491*, 752–755. https://doi.org/10.1038/nature11688

Choat, B., Sack, L., & Holbrook, N. M. (2007). Diversity of hydraulic traits in nine Cordia species growing in tropical forests with contrasting precipitation. *The New Phytologist*, *175*, 686–698. https://doi.org/10.1111/j.1469-8137.2007.02137.x

Collins, D. B. G., & Bras, R. L. (2007). Plant rooting strategies in water-limited ecosystems. *Water Resources Research*, *43*, 1–10. https://doi.org/10.1029/2006WR005541

Condon, L. E., & Maxwell, R. M. (2017). Systematic shifts in Budyko relationships caused by groundwater storage changes. *Hydrology and Earth System Sciences*, *21*, 1117–1135. https://doi.org/10.5194/hess-21-1117-2017

Cosme, L. H. M., Schietti, J., Costa, F. R. C., & Oliveira, R. S. (2017). The importance of hydraulic architecture to the distribution patterns of trees in a central Amazonian forest. *The New Phytologist*, *215*, 113–125. https://doi.org/10.1111/nph.14508

de Boer-Euser, T., McMillan, H. K., Hrachowitz, M., Winsemius, H. C., & Savenije, H. H. G. (2016). Influence of soil and climate on root zone storage capacity. *Water Resources Research*, *52*, 2009–2024. https://doi.org/10.1002/2015WR018115

De Cáceres, M., Martin-StPaul, N., Turco, M., Cabon, A., & Granda, V. (2018). Estimating daily meteorological data and downscaling climate models over landscapes. *Environmental Modelling & Software*, *108*, 186–196. https://doi.org/10.1016/j.envsoft.2018.08.003

De Cáceres, M., Martínez-Vilalta, J., Coll, L., Llorens, P., Casals, P., Poyatos, R., … Brotons, L. (2015). Coupling a water balance model with forest inventory data to predict drought stress: The role of forest structural changes vs. climate changes. *Agricultural and Forest Meteorology*, *213*, 77–90. https://doi.org/10.1016/j.agrformet.2015.06.012

del Castillo, J., Comas, C., Voltas, J., & Ferrio, J. P. (2016). Dynamics of competition over water in a mixed oak-pine Mediterranean forest: Spatio-temporal and physiological components. *Forest Ecology and Management*, *382*, 214–224. https://doi.org/10.1016/j.foreco.2016.10.025

DeLucia, E. H., Maherali, H., & Carey, E. V. (2000). Climate-driven changes in biomass allocation in pines. *Global Change Biology*, *6*, 587–593. https://doi.org/10.1046/j.1365-2486.2000.00338.x

Delzon, S., & Cochard, H. (2014). Recent advances in tree hydraulics highlight the ecological significance of the hydraulic safety margin. *The New Phytologist*, *203*, 355–358. https://doi.org/10.1111/nph.12798

Donohue, R. J., Roderick, M. L., & McVicar, T. R. (2012). Roots, storms and soil pores: Incorporating key ecohydrological processes into Budyko's hydrological model. *Journal of Hydrology*, *436–437*, 35–50. https://doi.org/10.1016/j.jhydrol.2012.02.033

Eagleson, P. S. (1982). Ecological optimality in water-limited natural soil-vegetation systems: 1. Theory and Hypothesis. *Water Resources Research*, *18*, 325–340. https://doi.org/10.1029/WR018i002p00325

Fan, Y., Miguez-Macho, G., Jobbágy, E. G., Jackson, R. B., Otero-Casal, C. (2017). Hydrologic regulation of plant rooting depth. *Proceedings of the National Academy of Sciences 114*, 201712381. https://doi.org/10.1073/pnas.1712381114, 10577

Federer, C. A., Vörösmarty, C., & Fekete, B. (2003). Sensitivity of annual evaporation to soil and root properties in two models of contrasting complexity. *Journal of Hydrometeorology*, *4*, 1276–1290. https://doi.org/10.1175/1525-7541(2003)004<1276:SOAETS>2.0.CO;2

Gao, H., Hrachowitz, M., Schymanski, S. J., Fenicia, F., Sriwongsitanon, N., & Savenije, H. H. G. (2014). Climate controls how ecosystems size the root zone storage capacity at catchment scale. *Geophysical Research Letters*, *41*, 7916–7923. https://doi.org/10.1002/2014GL061668

Gardner, W. R. (1964). Relation of root distribution to water uptake and availability. *Agronomy Journal*, *56*, 41. https://doi.org/10.2134/agronj1964.00021962005600010013x

Gracia, C., Ibàñez, J. J., Burriel, J. A., Mata, T., & Vayreda, J. (2004). *Inventari Ecològic i Forestal de Catalunya* (CREAF. ed.). Bellatera: CREAF.

Granier, A., Bréda, N., Biron, P., & Villette, S. (1999). A lumped water balance model to evaluate duration and intensity of drought constraints in forest stands. *Ecological Modelling*, *116*, 269–283. https://doi.org/10.1016/S0304-3800(98)00205-1

Granier, A., Reichstein, M., Bréda, N., Janssens, I. A., Falge, E., Ciais, P., … Wang, Q. (2007). Evidence for soil water control on carbon and water dynamics in European forests during the extremely dry year: 2003. *Agricultural and Forest Meteorology*, *143*, 123–145. https://doi.org/10.1016/j.agrformet.2006.12.004

Grier, C. C., & Running, S. W. (1977). Leaf area of mature northwestern coniferous forests: Relation to site water balance. *Ecology*, *58*, 893–899.

Guswa, A. J., Celia, M. A., & Rodriguez-Iturbe, I. (2004). Effect of vertical resolution on predictions of transpiration in water-limited ecosystems. *Advances in Water Resources*, *27*, 467–480. https://doi.org/10.1016/j.advwatres.2004.03.001

Hacke, U. G., Sperry, J. S., & Pittermann, J. (2000). Drought experience and cavitation resistance in six shrubs from the Great Basin, Utah. *Basic and Applied Ecology*, *1*, 31–41. https://doi.org/10.1078/1439-1791-00006

Hamer, J. J., Veneklaas, E. J., Renton, M., & Poot, P. (2016). Links between soil texture and root architecture of Eucalyptus species may limit distribution ranges under future climates. *Plant and Soil*, *403*, 217–229. https://doi.org/10.1007/s11104-015-2559-5

Hartmann, P., & von Wilpert, K. (2014). Fine-root distributions of Central European forest soils and their interaction with site and soil properties. *Canadian Journal of Forest Research*, *44*, 71–81. https://doi.org/10.1139/cjfr-2013-0357

Hoff, C., & Rambal, S. (2003). An examination of the interaction between climate, soil and leaf area index in a Quercus ilex ecosystem. *Annals of Forest Science*, *60*, 153–161. https://doi.org/10.1051/forest:2003008

Ibàñez, J. J., & Burriel, J. Á. (2010). Mapa de cubiertas del suelo de cataluña: características de la tercera edición y relación con siose. *Tecnol. la Inf. Geográfica La Inf. Geográfica al Serv. los Ciudad*, *3*, 179–198.

Ichii, K., Hashimoto, H., White, M. A., Potter, C., Hutyra, L. R., Huete, A. R., … Nemani, R. R. (2007). Constraining rooting depths in tropical rainforests using satellite data and ecosystem modeling for accurate simulation of gross primary production seasonality. *Global Change Biology*, *13*, 67–77. https://doi.org/10.1111/j.1365-2486.2006.01277.x

IPCC. (2014). Climate change 2014: Synthesis report. contribution of working groups I, II and III to the fifth assessment report of the intergovernmental panel on climate change., intergovernmental panel on climate change (IPCC) [core writing team, Pachauri, R.K. and Reisinger, A. (eds.)]. https://doi.org/10.1017/CBO9781107415324.004

Jackson, R. B., Canadell, J., Ehleringer, J. R., Mooney, H. a., Sala, O. E., & Schulze, E. D. (1996). A global analysis of root distributions for terrestrial biomes. *Oecologia*, *108*, 389–411. https://doi.org/10.1007/BF00333714

Jobbágy, E. G., & Jackson, R. B. (2001). The distribution of soil nutrients with depth: Global patterns and the imprint of plants. *Biogeochemistry*, *53*, 51–77. https://doi.org/10.1023/A:1010760720215

Joffre, R., Rambal, S., & Ratte, J. P. (1999). The dehesa system of southern Spain and Portugal as a natural ecosystem mimic. *Agroforestry Systems*, *45*, 57–79. https://doi.org/10.1023/A:1006259402496

Karavani, A., De Cáceres, M., Martínez de Aragón, J., Bonet, J. A., & De-Miguel, S. (2018). Effect of climatic and soil moisture conditions on mushroom productivity and related ecosystem services in Mediterranean pine stands facing climate change. *Agricultural and Forest Meteorology*, *248*, 432–440. https://doi.org/10.1016/j.agrformet.2017.10.024

Kergoat, L. (1998). A model for hydrological equilibrium of leaf area index on a global scale. *Journal of Hydrology*, *212–213*, 268–286. https://doi.org/10.1016/S0022-1694(98)00211-X

Kerkhoff, A. J., Martens, S. N., & Milne, B. T. (2004). An ecological evaluation of Eagleson's optimality hypotheses. *Functional Ecology*, *18*, 404–413. https://doi.org/10.1111/j.0269-8463.2004.00844.x

Kirchen, G., Calvaruso, C., Granier, A., Redon, P.-O., Van der Heijden, G., Bréda, N., & Turpault, M.-P. (2017). Local soil type variability controls the water budget and stand productivity in a beech forest. *Forest Ecology and Management*, *390*, 89–103. https://doi.org/10.1016/j.foreco.2016.12.024

Kleidon, A. (2004). Global datasets and rooting zone depth inferred from inverse methods. *Journal of Climate*, *17*, 2714–2722. https://doi.org/10.1175/1520-0442(2004)017<2714:GDORZD>2.0.CO;2

Kleidon, A., & Heimann, M. (1998). A method of determining rooting depth from a terrestrial biosphere model and its impacts on the global water and carbon cycle. *Global Change Biology*, *4*, 275–286. https://doi.org/10.1046/j.1365-2486.1998.00152.x

Laio, F., D'Odorico, P., & Ridolfi, L. (2006). An analytical model to relate the vertical root distribution to climate and soil properties. *Geophysical Research Letters*, *33*, 1–5. https://doi.org/10.1029/2006GL027331

Larter, M., Pfautsch, S., Domec, J. C., Trueba, S., Nagalingum, N., & Delzon, S. (2017). Aridity drove the evolution of extreme embolism resistance and the radiation of conifer genus Callitris. *The New Phytologist*, *215*, 97–112. https://doi.org/10.1111/nph.14545

Le Roux, P. C., Aalto, J., & Luoto, M. (2013). Soil moisture's underestimated role in climate change impact modelling in low-energy systems. *Global Change Biology*, *19*, 2965–2975. https://doi.org/10.1111/gcb.12286

Limousin, J. M., Rambal, S., Ourcival, J. M., Rodríguez-Calcerrada, J., Pérez-Ramos, I. M., Rodríguez-Cortina, R., … Joffre, R. (2012). Morphological and phenological shoot plasticity in a Mediterranean evergreen oak facing long-term increased drought. *Oecologia*, *169*, 565–577. https://doi.org/10.1007/s00442-011-2221-8

Llorens, P., Poyatos, R., Latron, J., Delgado, J., Oliveras, I., & Gallart, F. (2010). A multi-year study of rainfall and soil water controls on Scots pine transpiration under Mediterranean mountain conditions. *Hydrological Processes*, *24*, 3053–3064. https://doi.org/10.1002/hyp.7720

López, B., Sabaté, S., & Gracia, C. (1998). Fine roots dynamics in a Mediterranean forest: Effects of drought and stem density. *Tree Physiology*, *18*, 601–606. https://doi.org/10.1093/treephys/18.8-9.601

Lopez, O. R., Kursar, T. A., Cochard, H., & Tyree, M. T. (2005). Interspecific variation in xylem vulnerability to cavitation among tropical tree and shrub species. *Tree Physiology*, *25*, 1553–1562. https://doi.org/10.1093/treephys/25.12.1553

Manrique-Alba, À., Ruiz-Yanetti, S., Moutahir, H., Novak, K., De Luis, M., & Bellot, J. (2017). Soil moisture and its role in growth-climate relationships across an aridity gradient in semiarid Pinus halepensis forests. *Science of the Total Environment*, *574*, 982–990. https://doi.org/10.1016/j.scitotenv.2016.09.123

Martínez-Vilalta, J., Cochard, H., Mencuccini, M., Sterck, F., Herrero, A., Korhonen, J. F. J., … Zweifel, R. (2009). Hydraulic adjustment of Scots pine across Europe. *The New Phytologist*, *184*, 353–364. https://doi.org/10.1111/j.1469-8137.2009.02954.x

Maxwell, R. M., & Condon, L. E. (2016). Connections between groundwater flow and transpiration partitioning. *Science*, *353*(80), 377–380. https://doi.org/10.1126/science.aaf7891

McDowell, N. G., Beerling, D. J., Breshears, D. D., Fisher, R. A., Raffa, K. F., & Stitt, M. (2011). The interdependence of mechanisms underlying climate-driven vegetation mortality. *Trends in Ecology & Evolution*, *26*, 523–532. https://doi.org/10.1016/j.tree.2011.06.003

McDowell, N. G., Fisher, R. A., Xu, C., Domec, J. C., Hölttä, T., Mackay, D. S., … Pockman, W. T. (2013). Evaluating theories of drought-induced vegetation mortality using a multimodel-experiment framework. *The New Phytologist*, *200*, 304–321. https://doi.org/10.1111/nph.12465

Meinzer, F. C., Woodruff, D. R., Eissenstat, D. M., Lin, H. S., Adams, T. S., & McCulloh, K. A. (2013). Above-and belowground controls on water use by trees of different wood types in an eastern US deciduous forest. *Tree Physiology*, *33*, 345–356. https://doi.org/10.1093/treephys/tpt012

Mouillot, F., Rambal, S., & Lavorel, S. (2001). A generic process-based simulator for meditERRanean landscApes (SIERRA): Design and validation exercises. *Forest Ecology and Management*, *147*, 75–97. https://doi.org/10.1016/S0378-1127(00)00432-1

Nadal-Sala, D., Sabaté, S., & Gracia, C. (2013). GOTILWA+: un modelo de procesos que evalúa efectos del cambio climático en los bosques y explora alternativas de gestión para su mitigación. *Ecosistemas: Revista Cietifica Yy Tecnica de Ecologia Yy Medio Ambiente*, *22*, 29–36. https://doi.org/10.7818/856

Nardini, A., Casolo, V., Dal Borgo, A., Savi, T., Stenni, B., Bertoncin, P., … McDowell, N. G. (2016). Rooting depth, water relations and non-structural carbohydrate dynamics in three woody angiosperms differentially affected by an extreme summer drought. *Plant, Cell and Environment*, *39*, 618–627. https://doi.org/10.1111/pce.12646

Nemani, R. R., & Running, S. W. (1989). Testing a theoretical climate-soil-leaf area hydrologic equilibrium of forests using satellite data and ecosystem simulation. *Agricultural and Forest Meteorology*, *44*, 245–260. https://doi.org/10.1016/0168-1923(89)90020-8

Ninyerola, M., Pons, X., & Roure, J. M. (2000). A methodological approach of climatological modelling of air temperature and precipitation through GIS techniques. *International Journal of Climatology*, *20*, 1823–1841. https://doi.org/10.1002/1097-0088(20001130)20:14<1823::AID-JOC566>3.0.CO;2-B

Ogaya i Inurrigarro, R. (2004). *Plant ecophysiological responses to a field experimental drought in the Prades holm oak forest*. Universitat Autònoma de Barcelona.

Oren, R., & Pataki, D. E. (2001). Transpiration in response to variation in microclimate and soil moisture in southeastern deciduous forests. *Oecologia*, *127*, 549–559. https://doi.org/10.1007/s004420000622

Padilla, F. M., & Pugnaire, F. I. (2007). Rooting depth and soil moisture control Mediterranean woody seedling survival during drought. *Functional Ecology*, *21*, 489–495. https://doi.org/10.1111/j.1365-2435.2007.01267.x

Penman, H. L. (1948). Natural Evaporation from open water, bare soil and grass. *Proceedings of the Royal Society: A Mathemathical and Physical and Engineering Sciences*, *193*, 120–145. https://doi.org/10.1098/rspa.1948.0037

Piedallu, C., Gégout, J.-C., Perez, V., & Lebourgeois, F. (2013). Soil water balance performs better than climatic water variables in tree species distribution modelling. *Global Ecology and Biogeography*, *22*, 470–482. https://doi.org/10.1111/geb.12012

Pinheiro, H., DaMatta, F., Chaves, A., Loureiro, M., & Ducatti, C. (2005). Drought tolerance is associated with rooting depth and stomatal control of water use in clones of coffea canephora. *Annals of Botany*, *96*, 101–108. https://doi.org/10.1093/aob/mci154

Pivovaroff, A. L., Pasquini, S. C., De Guzman, M. E., Alstad, K. P., Stemke, J. S., & Santiago, L. S. (2016). Multiple strategies for drought survival among woody plant species. *Functional Ecology*, *30*, 517–526. https://doi.org/10.1111/1365-2435.12518

Pockman, W. T., & Sperry, J. S. (2000). Vulnerability to xylem cavitation and the distribution of Sonoran Desert Vegetation. *American Journal of Botany*, *87*, 1287–1299.

Poyatos, R., Aguadé, D., Galiano, L., Mencuccini, M., & Martínez-Vilalta, J. (2013). Drought-induced defoliation and long periods of near-zero gas exchange play a key role in accentuating metabolic decline of Scots pine. *The New Phytologist*, *200*, 388–401. https://doi.org/10.1111/nph.12278

Rodriguez-Iturbe, I., Porporato, A., Ridolfi, L., Isham, V., & Cox, D. R. (1999). Probabilistic modelling of water balance at a point: The role of climate, soil and vegetation. *Proceedings: Mathematical, Physical and Engineering on Sciences*, *455*, 3789–3805. https://doi.org/10.1098/rspa.1999.0477

Sarris, D., Christodoulakis, D., & Körner, C. (2007). Recent decline in precipitation and tree growth in the eastern Mediterranean. *Global Change Biology*, *13*, 1187–1200. https://doi.org/10.1111/j.1365-2486.2007.01348.x

Schenk, H. J. (2008). The shallowest possible water extraction profile: A null model for global root distributions. *Vadose Zone Journal*, *7*, 1119. https://doi.org/10.2136/vzj2007.0119

Schenk, H. J., & Jackson, R. B. (2002a). The global biogeography of roots. *Ecological Monographs*, *72*, 311. https://doi.org/10.2307/3100092

Schenk, H. J., & Jackson, R. B. (2002b). Rooting depths, lateral root spreads and belowground aboveground allometries of plants in water limited ecosystems. *Journal of Ecology*, *480–494*, 480–494. https://doi.org/10.1046/j.1365-2745.2002.00682.x

Schmid, I., & Kazda, M. (2002). Root distribution of Norway spruce in monospecific and mixed stands on different soils. *Forest Ecology and Management*, *159*, 37–47. https://doi.org/10.1016/S0378-1127(01)00708-3

Schulze, E.-D., Mooney, H. A., Sala, O. E., Jobbagy, E., Buchmann, N., Bauer, G., … Ehleringer, J. R. (1996). Rooting depth, water availability, and vegetation cover along an aridity gradient in Patagonia. *Oecologia*, *108*, 503–511. https://doi.org/10.1007/BF00333727

Schymanski, S. J., Sivapalan, M., Roderick, M. L., Beringer, J., & Hutley, L. B. (2008). An optimality-based model of the coupled soil moisture and root dynamics. *Hydrology and Earth System Sciences*, *12*, 913–932. https://doi.org/10.5194/hess-12-913-2008

Smettem, K., & Callow, N. (2014). Impact of forest cover and aridity on the interplay between effective rooting depth and annual runoff in South-West Western Australia. *Water*, *6*, 2539–2551. https://doi.org/10.3390/w6092539

Smettem, K. R. J., Waring, R. H., Callow, J. N., Wilson, M., & Mu, Q. (2013). Satellite-derived estimates of forest leaf area index in southwest Western Australia are not tightly coupled to interannual variations in rainfall: Implications for groundwater decline in a drying climate. *Global Change Biology*, *19*, 2401–2412. https://doi.org/10.1111/gcb.12223

Sperry, J. S., & Hacke, U. G. (2002). Desert shrub water relations with respect to soil characteristics and plant functional type. *Functional Ecology*, *16*, 367–378. https://doi.org/10.1046/j.1365-2435.2002.00628.x

Sperry, J. S., Hacke, U. G., Oren, R., & Comstock, J. P. (2002). Water deficits and hydraulic limits to leaf water supply. *Plant, Cell and Environment*, *25*, 251–263. https://doi.org/10.1046/j.0016-8025.2001.00799.x

Sperry, J. S., Wang, Y., Wolfe, B. T., Mackay, D. S., Anderegg, W. R. L., McDowell, N. G., & Pockman, W. T. (2016). Pragmatic hydraulic theory predicts stomatal responses to climatic water deficits. *The New Phytologist*, *212*, 577–589. https://doi.org/10.1111/NPH.14059

Stahl, C., Hérault, B., Rossi, V., Burban, B., Bréchet, C., & Bonal, D. (2013). Depth of soil water uptake by tropical rainforest trees during dry periods: Does tree dimension matter? *Oecologia*, *173*, 1191–1201. https://doi.org/10.1007/s00442-013-2724-6

Stone, E. L., & Kalisz, P. J. (1991). On the maximum extent of tree roots. *Forest Ecology and Management*, *46*, 59–102. https://doi.org/10.1016/0378-1127(91)90245-Q

Taufik, M., Torfs, P. J. J. F., Uijlenhoet, R., Jones, P. D., Murdiyarso, D., & Van Lanen, H. A. J. (2017). Amplification of wildfire area burnt by hydrological drought in the humid tropics. *Nature Climate Change*, *7*, 428–431. https://doi.org/10.1038/nclimate3280

Tietjen, B., Schlaepfer, D. R., Bradford, J. B., Lauenroth, W. K., Hall, S. A., Duniway, M. C., … Wilson, S. D. (2017). Climate change-induced vegetation shifts lead to more ecological droughts despite projected rainfall increases in many global temperate drylands. *Global Change Biology*, *23*, 2743–2754. https://doi.org/10.1111/gcb.13598

Tyree, M. T., & Sperry, J. S. (1988). Do Woody-plants operate near the point of catastrophic xylem dysfunction caused by dynamic water-stress—Answers from a model. *Plant Physiology*, *88*, 574–580. https://doi.org/10.1104/pp.88.3.574

Urli, M., Porte, A. J., Cochard, H., Guengant, Y., Burlett, R., & Delzon, S. (2013). Xylem embolism threshold for catastrophic hydraulic failure in angiosperm trees. *Tree Physiology*, *33*, 672–683. https://doi.org/10.1093/treephys/tpt030

van Wijk, M. T., & Bouten, W. (2001). Towards understanding tree root profiles: simulating hydrologically optimal strategies for root distribution. *Hydrology and Earth System Sciences*, *5*, 629–644. https://doi.org/10.5194/hess-5-629-2001

Wang-Erlandsson, L., Bastiaanssen, W. G. M., Gao, H., Jägermeyr, J., Senay, G. B., van Dijk, A. I. J. M., … Savenije, H. H. G. (2016). Global root zone storage capacity from satellite-based evaporation. *Hydrology and Earth System Sciences Discussions*, 1–49. https://doi.org/10.5194/hess-2015-533

Witty, J. H., Graham, R. C., Hubbert, K. R., Doolittle, J. A., & Wald, J. A. (2003). *Contributions of water supply from the weathered bedrock zone to forest soil quality* (Vol. 114, 114). (pp. 389, 389–400, 400). https://doi.org/10.1016/S0016-7061(03)00051-X

Wortemann, R., Herbette, S., Barigah, T. S., Fumanal, B., Alia, R., Ducousso, A., … Cochard, H. (2011). Genotypic variability and phenotypic plasticity of cavitation resistance in Fagus sylvatica L. across Europe. *Tree Physiology*, *31*, 1175–1182. https://doi.org/10.1093/treephys/tpr101

Zeng, X. B., Dai, Y. J., Dickinson, R. E., & Shaikh, M. (1998). The role of root distribution for climate simulation over land. *Geophysical Research Letters*, *25*, 4533–4536. https://doi.org/10.1029/1998GL900216

SUPPORTING INFORMATION

Additional supporting information may be found online in the Supporting Information section at the end of the article.

How to cite this article: Cabon A, Martínez-Vilalta J, Martínez de Aragón J, Poyatos R, De Cáceres M. Applying the eco-hydrological equilibrium hypothesis to model root distribution in water-limited forests. *Ecohydrology*. 2018;e2015. https://doi.org/10.1002/eco.2015